Pionic correlations and meson-exchange currents in two-particle emission induced by electron scattering

J. E. Amaro,[1] C. Maieron,[1] M. B. Barbaro,[2] J. A. Caballero,[3] and T. W. Donnelly[4]

[1]*Departamento de Física Atómica, Molecular y Nuclear, Universidad de Granada, E-Granada 18071, Spain*

[2]*Dipartimento di Fisica Teorica, Università di Torino and Istituto Nazionale di Fisica Nucleare, Sezione di Torino,
Via P. Giuria 1, I-10125 Torino, Italy*

[3]*Departamento de Física Atómica, Molecular y Nuclear, Universidad de Sevilla, Apdo. 1065, E-41080 Sevilla, Spain*

[4]*Center for Theoretical Physics, Laboratory for Nuclear Science and Department of Physics, Massachusetts Institute of Technology,
Cambridge, Massachusetts 02139, USA*

Two-particle two-hole contributions to electromagnetic response functions are computed in a fully relativistic Fermi gas model. All one-pion exchange diagrams that contribute to the scattering amplitude in perturbation theory are considered, including terms for pionic correlations and meson-exchange currents (MECs). The pionic correlation terms diverge in an infinite system and thus are regularized by modification of the nucleon propagator in the medium to take into account the finite size of the nucleus. The pionic correlation contributions are found to be of the same order of magnitude as the MECs.

I. INTRODUCTION

The goal of this article is to present a fully relativistic calculation of the two-particle two-hole (2p-2h) contributions to the inclusive (e, e') response functions of nuclei for intermediate to high momentum transfers in a Fermi gas model. Consistency with perturbation theory is maintained and all diagrams with one-pion exchange in the nuclear current are considered, constructed by attaching a photon to all possible lines in the basic one-pion exchange Feynman diagram. In this way not only meson-exchange currents (MECs) arise (for example, where the photon is attached to the pion), but also pionic correlation diagrams, where the virtual photon is absorbed by one of the two interacting nucleons. Both kinds of diagrams are considered in our model, together with the usual virtual Δ-isobar electroexcitation and decay.

We are motivated by previous work presented in Refs. [1,2], where only the MECs were included in the 2p-2h transverse (T) response, together with earlier work both in nonrelativistic [3] and relativistic [4–7] regimes. The contribution found from the 2p-2h excitations is small at the quasielastic (QE) peak, and increases with energy transfer, being more important in the dip region, where it is dominated by the Δ current. At the nonrelativistic level attempts were also made to evaluate the 2p-2h contribution of MECs in the T response for finite nuclei in a shell model [8,9].

The MECs are not the only two-body operators able to induce 2p-2h excitations. The correlation operators arising from Feynman diagrams where the photon is attached to a nucleon line, exchanging a pion with another nucleon, are of the same order as the MECs in the perturbative expansion and should be included to be consistent [10–12]. These diagrams, however, present the problem of giving an infinite answer in a Fermi gas model. The reason is that there is a nucleon propagator that can be on shell in the region of the quasielastic peak. Because the response function is the square of the amplitude, the resulting double pole gives an infinite result

after integration. In dealing with this problem, in Ref. [10] a prescription was followed by keeping the lines with a nucleon propagator strictly off the mass shell. A different approach was taken in Ref. [11] by subtracting from the proper self-energy its value on the mass shell, with the unphysical shortcoming of obtaining negative results for the 2p-2h responses to the left of the QE peak. Finally, in Ref. [12] a nucleon self-energy in the medium was introduced in the nucleon propagator. In dealing with the seven-dimensional integrals appearing in the 2p-2h responses, some of the previous calculations have resorted to the approximation of setting the two-hole momenta both equal to zero in some of the diagrams [10] or by taking into account only an average nucleon momentum [12].

In this work we revisit the double-pole problem to analyze the nature of the divergence of the resulting contributions. By isolating the divergent terms we are able to link them to the infinite extension of the Fermi gas system. In fact the double-pole term can be related to the probability of one-nucleon emission followed by nucleon rescattering off another nucleon, with the final ejection of two particles. This probability is infinite, because it is proportional to the propagation time of a real nucleon in a Fermi gas. This fact was pointed out in Ref. [12] where it was cured, as mentioned previously, by introducing a nucleon self-energy with an imaginary part giving it a finite lifetime for collisions. In this article we use a similar procedure by introducing a finite imaginary part $i\epsilon$ in the nucleon propagator, but with a new meaning for the free parameter ϵ. Instead of being an imaginary part of the nucleon self-energy for collisions, we relate it to the time T that a nucleon can travel across the nucleus before leaving it. Hence, this term accounts for the finite size of a real nucleus in contrast to an infinite system like the Fermi gas, where T is infinite. The value of ϵ can be estimated to be roughly about 200 MeV, appreciably larger than the usual values of the nucleon width for collisions.

The structure of this work is as follows. In Sec. II we present our model and define the 2p-2h response functions and the

two-body current operators. We discuss in depth the divergence of the correlation diagrams and the need to introduce the parameter ϵ in Sec. III (details of the numerical calculation are given in the appendixes). In Sec. IV we present results for the 2p-2h longitudinal and transverse response functions. In the case of the correlation diagrams we present results for several values of the parameter ϵ. Finally, in Sec. V we present our conclusions.

II. MODEL FOR 2P-2H RESPONSE FUNCTIONS

We consider an electron that scatters off a nucleus transferring four-momentum $Q^\mu = (\omega, \mathbf{q})$, with ω the energy transfer and $\mathbf{q}$ the momentum transfer. We follow closely the notation of Ref. [13]. Assuming plane waves for the electron, working in the laboratory system and taking the z direction along the momentum transfer, the inclusive cross section is written as

$$\frac{d\sigma}{d\Omega_e' d\omega} = \sigma_M [v_L R_L(q, \omega) + v_T R_T(q, \omega)], \tag{1}$$

where σ_M is the Mott cross section, v_L and v_T are the lepton kinematic factors, and the relevant quantities are the longitudinal $R_L(q, \omega)$ and transverse $R_T(q, \omega)$ response functions, respectively. These are defined as the following components of the hadronic tensor,

$$R_L = W^{00}, \tag{2}$$
$$R_T = W^{11} + W^{22}, \tag{3}$$

where

$$W^{\mu\nu} = \sum_f \langle f|J^\mu(Q)|i\rangle^* \langle f|J^\nu(Q)|i\rangle \delta(E_i + \omega - E_f), \tag{4}$$

and $J^\mu(Q)$ is the nuclear current operator.

In this article we take the initial nuclear state as the relativistic Fermi gas (RFG) model ground state, $|i\rangle = |F\rangle$, with all states with momenta below the Fermi momentum k_F occupied. The sum over final states can be decomposed as the sum of one-particle one-hole (1p-1h) plus two-particle two-hole (2p-2h) excitations plus additional channels. In the impulse approximation the 1p-1h channel gives the well-known response functions of the RFG. Here, we focus on the 2p-2h channel where the final states are of the type $|f\rangle = |\mathbf{p}_1' s_1', \mathbf{p}_2' s_2', \mathbf{h}_1^{-1} s_1, \mathbf{h}_2^{-1} s_2\rangle$, where $\mathbf{p}_i'$ are momenta of relativistic final nucleons above the Fermi sea, $p_i' > k_F$, with four-momenta $P_i' = (E_i', \mathbf{p}_i')$, and $H_i = (E_i, \mathbf{h}_i)$ are the four-momenta of the hole states with $h_i < k_F$. The spin indices are s_i' and s_i.

A. 2p-2h response functions

Because we have two species of nucleons, the 2p-2h responses can be further decomposed as the sum of two-proton (PP), two-neutron (NN), and proton-neutron (PN) emission,

$$R_K = R_K(PP) + R_K(NN) + R_K(PN). \tag{5}$$

For the PP channel we write down the L response as (likewise for the T response):

$$R_L(PP) = \frac{1}{4} \sum_{\mathbf{p}_1' s_1'} \sum_{\mathbf{p}_2' s_2'} \sum_{\mathbf{h}_1 s_1} \sum_{\mathbf{h}_2 s_2} \left| \langle \mathbf{p}_1' \mathbf{p}_2' \mathbf{h}_1^{-1} \mathbf{h}_2^{-1} | J^0(Q) | F \rangle \right|^2$$
$$\times \delta(E_1' + E_2' - \omega - E_1 - E_2), \tag{6}$$

where the spin indices are implicit in the matrix elements. The factor $\frac{1}{4}$ comes from antisymmetry of the wave functions, to avoid double counting of the final states under the interchange of the indices $1' \leftrightarrow 2'$ and $1 \leftrightarrow 2$. Exploiting the antisymmetry, the many-body matrix element of a two-body operator can be written as the direct minus exchange part of the two-body current matrix element,

$$\langle \mathbf{p}_1' \mathbf{p}_2' \mathbf{h}_1^{-1} \mathbf{h}_2^{-1} | J^\mu | F \rangle = \langle \mathbf{p}_1' \mathbf{p}_2' | J^\mu | \mathbf{h}_1 \mathbf{h}_2 \rangle - \langle \mathbf{p}_1' \mathbf{p}_2' | J^\mu | \mathbf{h}_2 \mathbf{h}_1 \rangle,$$

which we write in terms of the two-body current function $j^\mu(\mathbf{p}_1', \mathbf{p}_2', \mathbf{h}_1, \mathbf{h}_2)$ to be specified below,

$$\langle \mathbf{p}_1' \mathbf{p}_2' | J^\mu | \mathbf{h}_1 \mathbf{h}_2 \rangle = (2\pi)^3 \delta(\mathbf{p}_1' + \mathbf{p}_2' - \mathbf{h}_1 - \mathbf{h}_2 - \mathbf{q})$$
$$\times \frac{m^2}{V^2 (E_1 E_2 E_1' E_2')^{1/2}} j^\mu(\mathbf{p}_1', \mathbf{p}_2', \mathbf{h}_1, \mathbf{h}_2). \tag{7}$$

Going to the thermodynamic limit and integrating over the momentum $\mathbf{p}_2'$ we obtain

$$R_L(PP) = \frac{V}{4} \sum_{s_1' s_2' s_1 s_2} \int \frac{d^3 p_1'}{(2\pi)^3} \frac{d^3 h_1}{(2\pi)^3} \frac{d^3 h_2}{(2\pi)^3}$$
$$\times \frac{m^4}{E_1 E_2 E_1' E_2'} |j^0(\mathbf{p}_1', \mathbf{p}_2', \mathbf{h}_1, \mathbf{h}_2)_A|^2$$
$$\times \delta(E_1' + E_2' - \omega - E_1 - E_2)\theta(p_2' - k_F), \tag{8}$$

where $\mathbf{p}_2' = \mathbf{h}_1 + \mathbf{h}_2 + \mathbf{q} - \mathbf{p}_1'$, and the integration limits are $h_1, h_2 < k_F$, $p_1' > k_F$. We have defined the antisymmetrized current function,

$$j^\mu(1', 2', 1, 2)_A \equiv j^\mu(1', 2', 1, 2) - j^\mu(1', 2', 2, 1),$$

with obvious meaning for the abbreviated arguments. Expanding the square inside the integral in Eq. (8), three terms are obtained:

$$|j^\mu(1', 2', 1, 2)_A|^2 = |j^\mu(1', 2', 1, 2)|^2 + |j^\mu(1', 2', 2, 1)|^2$$
$$- 2\text{Re } j^\mu(1', 2', 2, 1)^* j^\mu(1', 2', 1, 2). \tag{9}$$

Changing variables $1 \leftrightarrow 2$ in the second term under the integral, we obtain the first term again. Hence we can finally write for the PP response,

$$R_L(PP) = \frac{V}{2} \sum_{s_1' s_2' s_1 s_2} \int \frac{d^3 p_1'}{(2\pi)^3} \frac{d^3 h_1}{(2\pi)^3} \frac{d^3 h_2}{(2\pi)^3}$$
$$\times \frac{m^4}{E_1 E_2 E_1' E_2'} [|j^0(\mathbf{p}_1', \mathbf{p}_2', \mathbf{h}_1, \mathbf{h}_2)|^2$$
$$- \text{Re } j^0(\mathbf{p}_1', \mathbf{p}_2', \mathbf{h}_1, \mathbf{h}_2)^* j^0(\mathbf{p}_1', \mathbf{p}_2', \mathbf{h}_2, \mathbf{h}_1)]$$
$$\times \delta(E_1' + E_2' - \omega - E_1 - E_2)\theta(p_2' - k_F). \tag{10}$$

Note that the factor $\frac{1}{2}$ in front of the sum comes from the antisymmetry of the particles (protons). A similar expression is obtained for the NN response $R_L(NN)$. In the case of the PN channel we subtract the charge exchange contribution without any symmetry term because there are no additional isospin sums, and the result is

$$
\begin{aligned}
R_L(PN) = V \sum_{s_1' s_2' s_1 s_2} \int & \frac{d^3 p_1'}{(2\pi)^3} \frac{d^3 h_1}{(2\pi)^3} \frac{d^3 h_2}{(2\pi)^3} \\
\times & \frac{m^4}{E_1 E_2 E_1' E_2'} |\langle PN|j^0(\mathbf{p}_1', \mathbf{p}_2', \mathbf{h}_1, \mathbf{h}_2)|PN\rangle \\
& - \langle NP|j^0(\mathbf{p}_1', \mathbf{p}_2', \mathbf{h}_2, \mathbf{h}_1)|PN\rangle|^2 \\
\times & \delta(E_1' + E_2' - \omega - E_1 - E_2)\theta(p_2' - k_F).
\end{aligned}
\tag{11}
$$

Finally, note that the 2p-2h response is proportional to the volume of the system V which is related to the number of particles $\mathcal{N}$ (protons or neutrons) by $V = 3\pi^2 \mathcal{N}/k_F^3$.

B. Two-body current matrix elements

The MECs considered in this work are represented by the Feynman diagrams of Fig. 1. The pionic four-momenta K_1, K_2 are defined via $K_i^\mu = P_i'^\mu - H_i^\mu$ as the four-momenta given to the nucleons 1 and 2, respectively, by the exchanged pion.

Assuming pseudovector nucleon-pion coupling, the fully relativistic two-body current matrix elements are given by [13,14]

(i) (a) and (b) Seagull or contact:

$$
\begin{aligned}
j_s^\mu(\mathbf{p}_1', \mathbf{p}_2', \mathbf{p}_1, \mathbf{p}_2) = & \frac{f^2}{m_\pi^2} i\epsilon_{3ab} \bar{u}(\mathbf{p}_1')\tau_a \gamma_5 \, K\!\!\!/_1 u(\mathbf{p}_1) \\
& \times \frac{F_1^V}{K_1^2 - m_\pi^2} \bar{u}(\mathbf{p}_2')\tau_b \gamma_5 \gamma^\mu u(\mathbf{p}_2) \\
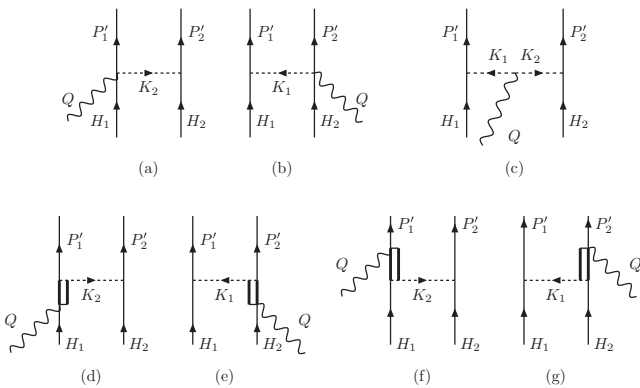& + (1 \leftrightarrow 2).
\end{aligned}
\tag{12}
$$

FIG. 1. MEC diagrams considered in the present study. Diagrams (a) and (b) correspond to the seagull, (c) to the pionic, and (d)–(g) to the Δ current, respectively.

(ii) (c) Pion in flight:

$$
\begin{aligned}
& j_p^\mu(\mathbf{p}_1', \mathbf{p}_2', \mathbf{p}_1, \mathbf{p}_2) \\
& = \frac{f^2}{m_\pi^2} i\epsilon_{3ab} \frac{F_\pi (K_1 - K_2)^\mu}{(K_1^2 - m_\pi^2)(K_2^2 - m_\pi^2)} \bar{u}(\mathbf{p}_1')\tau_a \gamma_5 \, K\!\!\!/_1 \\
& \times u(\mathbf{p}_1)\bar{u}(\mathbf{p}_2')\tau_b \gamma_5 \, K\!\!\!/_2 u(\mathbf{p}_2).
\end{aligned}
\tag{13}
$$

In the previous expressions we use the Einstein convention for the sum over a repeated isospin index $a = 1, 2, 3$. Moreover, F_1^V and F_π are the electromagnetic isovector nucleon and pion form factors, respectively. The spinors are normalized according to the Bjorken and Drell convention [15] and the pion-nucleon coupling constant is $f^2/4\pi = 0.08$.

(iii) (d)–(g) Δ current:

$$
\begin{aligned}
& j_\Delta^\mu(\mathbf{p}_1', \mathbf{p}_2', \mathbf{p}_1, \mathbf{p}_2) \\
& = \frac{f_{\pi N \Delta} f}{m_\pi^2} \frac{1}{K_2^2 - m_\pi^2} \bar{u}(\mathbf{p}_1') T_a^\mu(1) u(\mathbf{p}_1) \\
& \times \bar{u}(\mathbf{p}_2')\tau_a \gamma_5 \, K\!\!\!/_2 u(\mathbf{p}_2) + (1 \leftrightarrow 2).
\end{aligned}
\tag{14}
$$

The vector $T_a^\mu(1)$ is related to the pion electroproduction amplitude,

$$
\begin{aligned}
T_a^\mu(1) = & K_{2,\alpha}\Theta^{\alpha\beta} G_{\beta\rho}^\Delta(H_1 + Q) S_f^{\rho\mu}(H_1) T_a T_3^\dagger \\
& + T_3 T_a^\dagger S_b^{\mu\rho}(P_1') G_{\rho\beta}^\Delta(P_1' - Q)\Theta^{\beta\alpha} K_{2,\alpha}.
\end{aligned}
\tag{15}
$$

The forward Δ electroexcitation tensor is[1]

$$
\begin{aligned}
S_f^{\rho\mu}(H_1) = & \Theta^{\rho\mu}[g_1 \, Q\!\!\!/ - g_2 H_1 \cdot Q + g_3 Q^2]\gamma_5 \\
& - \Theta^{\rho\nu} Q_\nu [g_1 \gamma^\mu - g_2 H_1^\mu + g_3 Q^\mu]\gamma_5,
\end{aligned}
\tag{16}
$$

and the backward tensor amplitude is

$$
\begin{aligned}
S_b^{\rho\mu}(P_1') = & \gamma_5[g_1 \, Q\!\!\!/ - g_2 P_1' \cdot Q - g_3 Q^2]\Theta^{\mu\rho} \\
& - \gamma_5 [g_1 \gamma^\mu - g_2 P_1'^\mu - g_3 Q^\mu] Q_\nu \Theta^{\nu\rho}.
\end{aligned}
\tag{17}
$$

The tensor $\Theta_{\mu\nu}$ is defined by

$$
\Theta_{\mu\nu} = g_{\mu\nu} - \frac{1}{4}\gamma_\mu \gamma_\nu.
\tag{18}
$$

For the Δ propagator we use the usual Rarita-Schwinger (RS) tensor,

$$
\begin{aligned}
G_{\beta\rho}^\Delta(P) = & -\frac{P\!\!\!/ + m_\Delta}{P^2 - m_\Delta^2}\left[g_{\beta\rho} - \frac{1}{3}\gamma_\beta \gamma_\rho - \frac{2}{3}\frac{P_\beta P_\rho}{m_\Delta^2}\right. \\
& \left. - \frac{\gamma_\beta P_\rho - \gamma_\rho P_\beta}{3m_\Delta}\right].
\end{aligned}
\tag{19}
$$

In what follows we perform the substitution $m_\Delta \to m_\Delta + \frac{i}{2}\Gamma(P)$ in the denominator of the propagator to account for the Δ decay probability. Finally, the electromagnetic coupling constants g_i are given by

$$
g_1 = \frac{G_1}{2m_N}, \quad g_2 = \frac{G_2}{4m_N^2}, \quad g_3 = \frac{G_3}{4m_N^2}.
\tag{20}
$$

_____

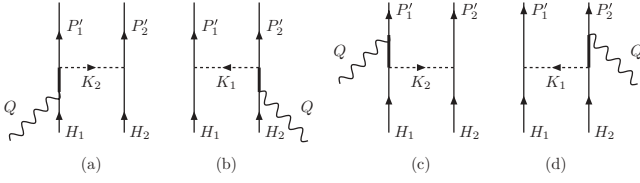[1]Note that there is a sign error in Eq. (15) of [14].

FIG. 2. Correlation diagrams considered in the present study. Diagrams (a) and (b) correspond to the forward, and (c) and (d) backward contributions, respectively.

Our approach for the Δ follows, as a particular case, from the more general form of the $\gamma N \Delta$ Lagrangian of Pascalutsa *et al.* [16]. The Δ coupling constants used here are $G_1 = 4.2$, $G_2 = 4$, $G_3 = 1$, and $f_{\pi N \Delta} = 4 \times 0.564$.

The correlation current is defined in Fig. 2, and given by

$$
\begin{aligned}
j_{\text{cor}}^{\mu}(\mathbf{p}_1', \mathbf{p}_2', \mathbf{p}_1, \mathbf{p}_2) = {} & \frac{f^2}{m_\pi^2} \bar{u}(\mathbf{p}_1') \tau_a \gamma_5 \not{K}_1 u(\mathbf{p}_1) \frac{1}{K_1^2 - m_\pi^2} \\
& \times \bar{u}(\mathbf{p}_2')[\tau_a \gamma_5 \not{K}_1 S_F(P_2 + Q)\Gamma^\mu(Q) \\
& + \Gamma^\mu(Q) S_F(P_2' - Q)\tau_a \gamma_5 \not{K}_1]u(\mathbf{p}_2) \\
& + (1 \leftrightarrow 2),
\end{aligned}
\tag{21}
$$

where $S_F(P)$ is the Feynman propagator for the nucleon,

$$
S_F(P) = \frac{\not{P} + m}{P^2 - m^2 + i\epsilon},
\tag{22}
$$

and $\Gamma^\mu(Q)$ is the electromagnetic nucleon vertex,

$$
\Gamma^\mu(Q) = F_1 \gamma^\mu + \frac{i}{2m} F_2 \sigma^{\mu\nu} Q_\nu.
\tag{23}
$$

The nucleon form factors F_1 and F_2 are given by the Galster parametrization [17].

The isospin sums and isospin matrix elements must be performed separately for each isospin channel. Explicit expressions are given in Appendix A.

III. DIVERGENCE OF THE CORRELATION RESPONSES

The response functions computed using the correlation current in Eq. (21) are divergent in the Fermi gas. There are two sources for this divergence: the first one comes from the double pole of the propagator when taking the square of the current. This divergence can be shown to behave as $1/\epsilon$ plus principal value terms going as $\log \epsilon$. The second source is related to the behavior of the principal values arising from the double and single poles near the RFG boundary of the quasielastic peak, where the principal values present a logarithmic divergence.

To illustrate the mathematical structure of this divergence we isolate as an example the singularities produced by the diagram of Fig. 2(a). The corresponding current operator can be written as

$$
j^\mu = \frac{l^\mu}{E_1 + \omega - E_{\mathbf{h}_1 + \mathbf{q}} + i\epsilon},
\tag{24}
$$

where $E_{\mathbf{p}} = \sqrt{m^2 + \mathbf{p}^2}$ is the on-shell energy. We have explicitly extracted the divergent part of the denominator, with

a pole for

$$
E_{\mathbf{h}_1 + \mathbf{q}} = E_1 + \omega,
\tag{25}
$$

in the limit $\epsilon \to 0$. The previous equation is equivalent to the quasielastic condition for emission of an on-shell nucleon with four-momentum $H_1 + Q$. In fact, for a given value of h_1, Eq. (25) holds when the angle between $\mathbf{h}_1$ and $\mathbf{q}$ is given by

$$
\cos\theta_1 = \frac{Q^2 + 2E_1\omega}{2h_1 q}.
\tag{26}
$$

Because the condition $-1 < \cos\theta_1 < 1$ defines the boundary of the quasielastic peak, the pole can always be reached in that region.

To study the behavior of the response functions from this pole, it is convenient to change the variable θ_1 to a new variable defined by

$$
x_1 \equiv E_1 + \omega - E_{\mathbf{h}_1 + \mathbf{q}},
\tag{27}
$$

in the integral over $\mathbf{h}_1$ in Eq. (10). Then the components of the total current matrix element can be written as a function of x_1 in the general form,

$$
f(x_1) = \frac{\varphi(x_1)}{x_1 + i\epsilon} + g(x_1),
\tag{28}
$$

where the first term comes from diagram 2(a) and the function $g(x_1)$ comes from the sum of the remaining diagrams, and is finite for $x_1 = 0$. Because the current appears squared in the response function, we are dealing with the integral of a function of the kind,

$$
|f(x_1)|^2 = \frac{|\varphi(x_1)|^2}{x_1^2 + \epsilon^2} + |g(x_1)|^2 + 2\text{Re} \frac{\varphi^*(x_1)g(x_1)}{x_1 - i\epsilon}.
\tag{29}
$$

When integrating this function over x_1, and taking the limit $\epsilon \to 0$, the first term has a double pole for $x_1 = 0$, whereas the third one has a single pole. To deal with the single pole we use the usual Plemeli relation,

$$
\frac{1}{x + i\epsilon} = \mathcal{P}\frac{1}{x} - i\pi\delta(x).
\tag{30}
$$

To apply a similar relation for the double pole term, we add and subtract the on-shell value $|\varphi(0)|^2/(x_1^2 + \epsilon^2)$. Taking the limit $\epsilon \to 0$ we can use relations that are valid for any function $\psi(x)$,

$$
\int_{-a}^{b} \frac{\psi(x) - \psi(0)}{x^2 + \epsilon^2} dx \to \mathcal{P}\int_{-a}^{b} \frac{\psi(x) - \psi(0)}{x^2} dx,
\tag{31}
$$

and

$$
\int_{-a}^{b} \frac{\psi(0)}{x^2 + \epsilon^2} dx = \frac{1}{\epsilon}\left[\tan^{-1}\frac{b}{\epsilon} + \tan^{-1}\frac{a}{\epsilon}\right]\psi(0) \sim \frac{\pi}{\epsilon}\psi(0).
\tag{32}
$$

Then Eq. (29) can be written in the form,

$$
\begin{aligned}
|f(x_1)|^2 = {} & \mathcal{P}\frac{|\varphi(x_1)|^2 - |\varphi(0)|^2}{x_1^2} + |g(x_1)|^2 \\
& + 2\mathcal{P}\frac{\text{Re}\,\varphi^*(x_1)g(x_1)}{x_1} - 2\pi\,\text{Im}\,\varphi^*(0)g(0)\delta(x_1) \\
& + \frac{|\varphi(0)|^2}{\epsilon}\pi\delta(x_1).
\end{aligned}
\tag{33}
$$

The last $O(1/\epsilon)$ term in Eq. (33) provides the dominant contribution to the response function, being infinite for $\epsilon \to 0$. Because of the δ function, that term does not contribute outside the quasielastic-peak region, where x_1 is different from zero.

The principal values present in Eq. (33) also diverge in the particular case in which one of the limits of integration is zero. In that case, the principal value in Eq. (30) should be computed instead using

$$\mathcal{P}\int_{-a}^{b} \frac{\psi(x)}{x}dx = \int_{-a}^{b} \frac{\psi(x) - \psi(0)}{x}dx + \frac{1}{2}\psi(0)\ln\frac{b^2 + \epsilon^2}{a^2 + \epsilon^2},$$
(34)

and it gives a $\ln\epsilon$ term if a or b is zero. That situation, in fact, occurs throughout the quasielastic region, and in particular at the boundary of the quasielastic peak. Therefore one expects an additional divergence $\sim O(\ln\epsilon)$.

The meaning of the term $\frac{|\varphi(0)|^2}{\epsilon}\pi\delta(x_1)$ is explained in what follows. Diagram 2(a), when the intermediate nucleon is on shell, gives the probability of a 1p-1h electroexcitation times the probability of quasielastic nucleon scattering. Because the interaction probability is proportional to the interaction time T, the probability of this rescattering process is proportional to T^2. Therefore, the cross section is proportional to T. In an infinite system such as the Fermi gas, the intermediate nucleon never leaves the nucleus and therefore $T \to \infty$. However, in a finite nucleus one expects no divergence because a high-energy nucleon will leave the nucleus in a finite time. Therefore, the interaction time is finite.

The relation between ϵ and T can also be obtained by inspection of the momentum-space propagator in quantum field theory [18], computed as the vacuum expectation value of time-ordered Fermion fields. The value ϵ in the denominator of the propagator can be seen as a regularization parameter in the Fourier transform of the time-step function for a particle with four-momentum $P^\mu = (p_0, \mathbf{p})$,

$$\int_{-T/2}^{T/2} dt\, e^{i(p_0 - E_\mathbf{p})t}\theta(t) = \frac{i}{p_0 - E_\mathbf{p} + i\epsilon},$$
(35)

where $T \to \infty$ and $\epsilon \to 0$. For a real particle, $p_0 - E_\mathbf{p} = 0$, the left-hand side of the above equation is $T/2$, and the right-hand side is $1/\epsilon$. Therefore,

$$\frac{T}{2} = \frac{1}{\epsilon}.$$
(36)

In this article we cure the divergence of the correlation diagram by a regularization procedure, using a finite value for ϵ to account for the finite propagation time of a high-energy nucleon in a nucleus before leaving it. To estimate the value of ϵ for a nucleus such as ^{12}C, we assume that the nucleon moves at the velocity of light and it has to cross a distance equal to the nuclear radius $R \sim 2$ fm. Then,

$$\epsilon \simeq \frac{2\hbar}{T} \simeq \frac{2\hbar c}{R} \simeq \frac{400}{2}\text{MeV} \simeq 200\,\text{MeV}.$$
(37)

Note that this value, $\epsilon \simeq 200$ MeV, is very different from the nucleon width $\Gamma \sim 10$ MeV which is usually obtained in nuclear matter as the width for nuclear inelastic interaction. In practice, the value of ϵ can be taken as a parameter to be

fitted to data. In the next section we perform a study of the dependence of our results upon ϵ. Unless otherwise specified we assume $\epsilon = 200$ MeV.

At this point we should mention that the use of Eq. (29) to compute the 2p-2h response functions becomes impractical because of complications in the numerical calculation of principal values in multidimensional integrals including the four diagrams of Fig. 2 (and the corresponding exchange parts). Because we are forced to use a finite value of ϵ, it becomes more convenient to keep from the beginning the $i\epsilon$ term in the denominator of the nucleon propagator in Eq. (21).

IV. RESULTS

Here we present results for the longitudinal and transverse response functions for inclusive two-particle emission. We compute the 2p-2h response functions in the RFG model as the nine-dimensional (9D) integrals given by Eqs. (10) and (11). The energy δ function can be used to integrate over p_1', fixing the energy E_1' of the first particle. More details are given in
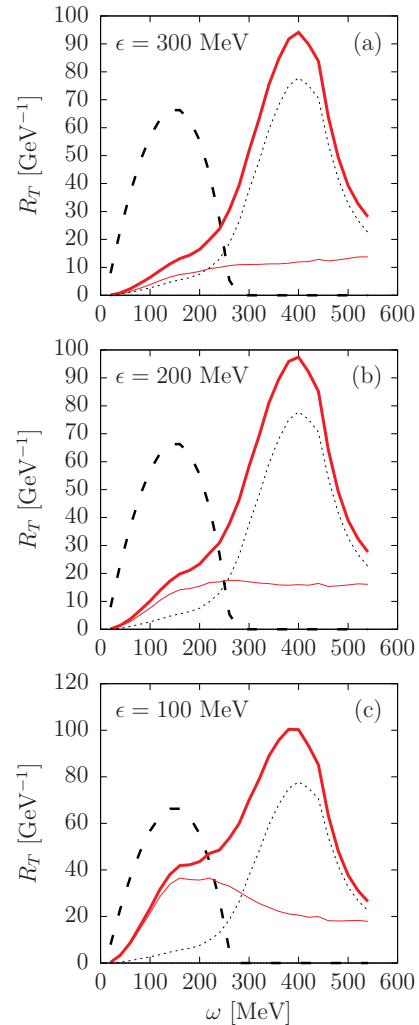

FIG. 3. (Color online) 2p-2h transverse response of ^{56}Fe at $q = 550$ MeV/c. Three values of the parameter ϵ are shown. Thin solid lines, correlation only; dotted lines, MECs only; thick solid lines, total; dashed, RFG OB results.

Appendix B. By rotational invariance considerations, one of the azimuthal angles can be fixed, multiplying at the same time the result by a factor 2π. We choose $\phi_1' = 0$. At the end we have a seven-dimensional integration to be performed numerically. The usual procedure is to use a multidimensional Monte Carlo (MC) integration. Because the pole structure of the integrand is numerically delicate, in this work we use instead a mixed Monte Carlo–Simpson integration procedure. The Simpson algorithm is used for integration over the angles of the two holes θ_1, θ_2 and of the first particle θ_1'. The remaining four-dimensional integral over the hole momenta h_1, h_2 and their angles ϕ_1, ϕ_2 is made by Monte Carlo. To keep the CPU times manageable we use a number of MC points of the order of 10^3 for $q = 1$ GeV/c. For other values of the momentum transfer the number of MC points is modified linearly with q. We have performed a study of the stability of the results with the number of MC points and have found that the error from the integration procedure is within a few percent.

A pion-nucleon form factor is included in the two-body currents: $F_{\pi NN}(K_\pi) = (\Lambda^2 - m_\pi^2)/(\Lambda^2 - K_\pi^2)$, with $\Lambda = 1.3$ GeV. We use the same value for the $\pi N \Delta$ form factor

in the Δ current. The electromagnetic form factors are those of Galster for the nucleon, and those used in Refs. [13,14] for the MECs.

To make contact with previous work, we apply our model to compute the 2p-2h longitudinal and transverse response functions for the nucleus ^{56}Fe, and for momenta $q = 550$ and 1140 MeV/c. The results are presented in Figs. 3–6, where the separate contributions of the correlation and MECs to the 2p-2h responses are also shown. The 1p-1h responses produced by the one-body (OB) current in the relativistic Fermi gas without interaction are also shown.

A critical input for our model is the value of the parameter ϵ in the nucleon propagator, introduced to cure the divergence of the double pole. To see how the responses for the correlation contribution depend on ϵ we show results for three different values: $\epsilon = 100, 200$, and 300 MeV. For $\epsilon = 100$ MeV, the correlation 2p-2h contribution presents a shape with a maximum in the region of the quasielastic peak, but with a long tail extended to high transferred energies. The maximum is reminiscent of the pole structure of the nucleon propagator, and therefore a resonance appears for kinematics corresponding
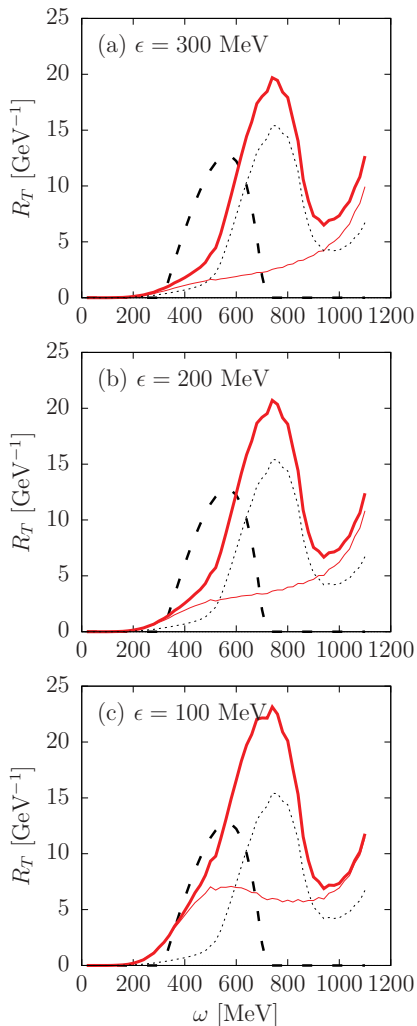

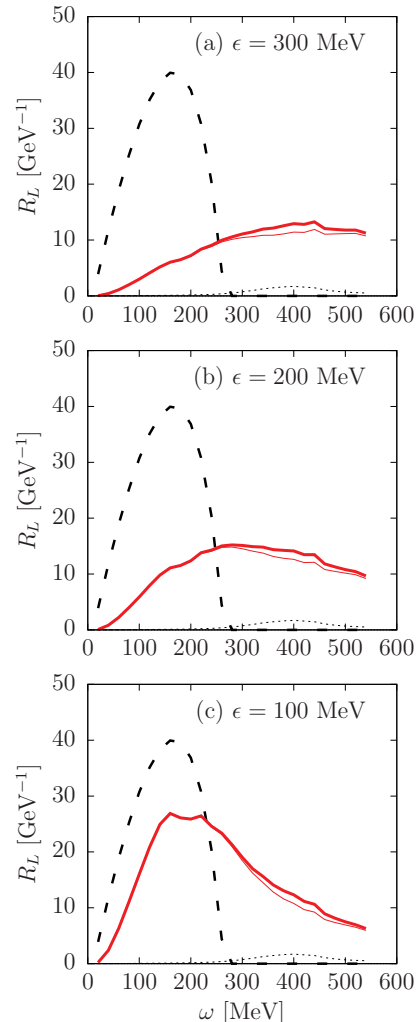FIG. 4. (Color online) The same as for Fig. 3, but now at $q = 1140$ MeV/c.

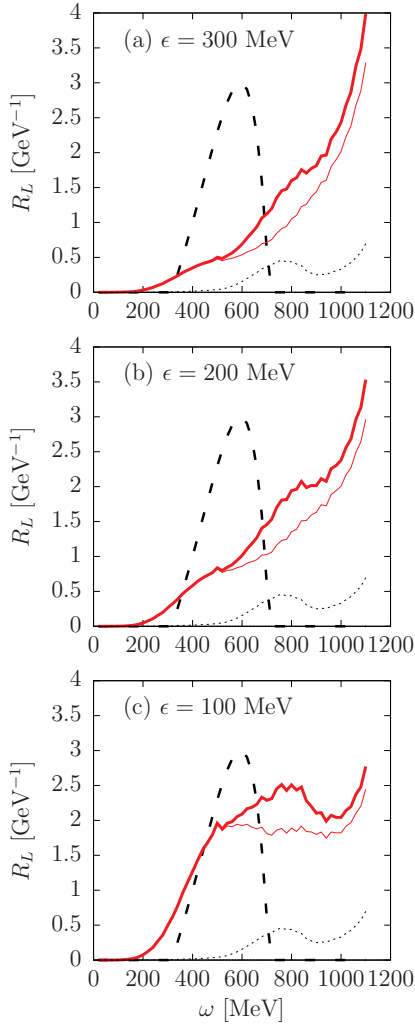FIG. 5. (Color online) The same as for Fig. 3, but now for R_L.

FIG. 6. (Color online) The same as for Fig. 3, but now for R_L at $q = 1140$ MeV/c.

FIG. 7. (Color online) 2p-2h correlation contribution to the L and T responses of ^{56}Fe for $q = 550$ MeV/c. Three values of the parameter ϵ are shown. With dotted lines from up to down, $\epsilon = 100$, 200, 300, respectively. Solid lines, RFG one-body responses.

to the quasielastic condition in Eq. (26). A shift to higher energies (of the order of ~ 40 MeV) is seen in the case of $q = 550$ MeV/c (Figs. 3 and 5). Indeed for this value of q the phase space for two-particle emission causes a suppression of the low-energy side of the response function.

The resonant structure produced by the 2p-2h correlation contribution diminishes significantly with increasing values of the parameter ϵ. Notice that for $\epsilon \geqslant 200$ MeV there is no maximum located at the QE peak.

For an even lower value of the escape width, say $\epsilon = 50$ MeV, the magnitude of the resonant peak is of the same size as the OB response function. This correction coming from 2p-2h states is obviously too large to be compatible with experimental data that are already of the order of the 1p-1h response at the region of the QE peak. It should be mentioned that, although the 2p-2h contribution should be added to the 1p-1h one, the latter should be first corrected for final-state interaction (FSI) contributions not included in the bare RFG results shown in the figures. In fact, FSIs contribute importantly to one-nucleon emission through the coupling of 1p-1h to 2p-2h states in the final nucleus [19]. These processes
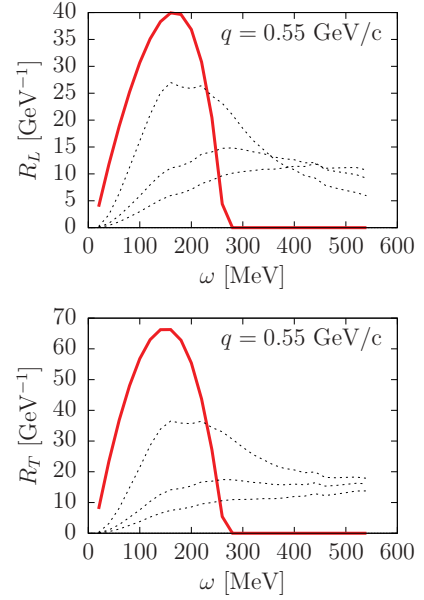
involve, in particular, two-pion exchange, and are, therefore, of the same order as the 2p-2h response in the perturbative series because it is the square of one-pion exchange matrix element. The inclusion of such contributions is out of the scope of the present study.

The dependence of the correlation responses on the parameter ϵ is better appreciated in Figs. 7 and 8, where we show its contribution for the three chosen values of ϵ in the same plot. In the QE region the height of the responses approximately reduces to one-half when ϵ doubles. This behavior follows
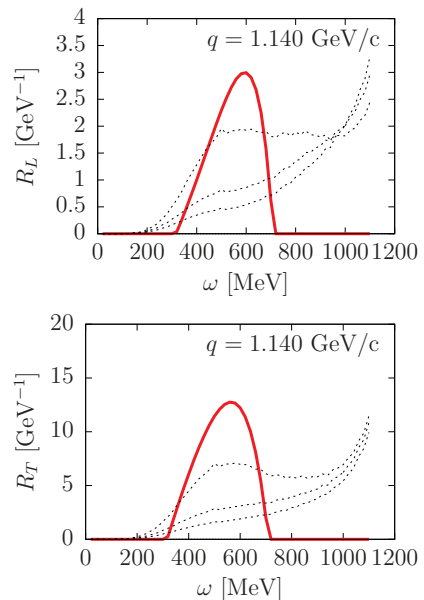

FIG. 8. (Color online) The same as for Fig. 7, but now at $q = 1140$ MeV/c.

because of the leading $1/\epsilon$ dependence in Eq. (33), coming from the pole in the propagator. For high ω the results are more similar and they are almost independent of ϵ in the high-energy tail. In this case (i.e., large ω), there is no pole in the integrand and the contribution from the propagator is less sensitive to the precise value of ϵ.

Let us return now to Figs. 3–6, where the MEC separate contribution is also shown. The transverse response (Figs. 3 and 4) has a large peak with a maximum around $\omega = (m_\Delta^2 + q^2)^{1/2} - m_N$ that comes from the Δ propagator appearing in the Δ current. It has the same resonant structure as the correlation current, but located in the region of the Δ peak, where the real pion emission cross section has a maximum. We do not include the pion emission channel in our calculation. Both channels should be summed up to obtain the total inclusive (e, e') cross section.
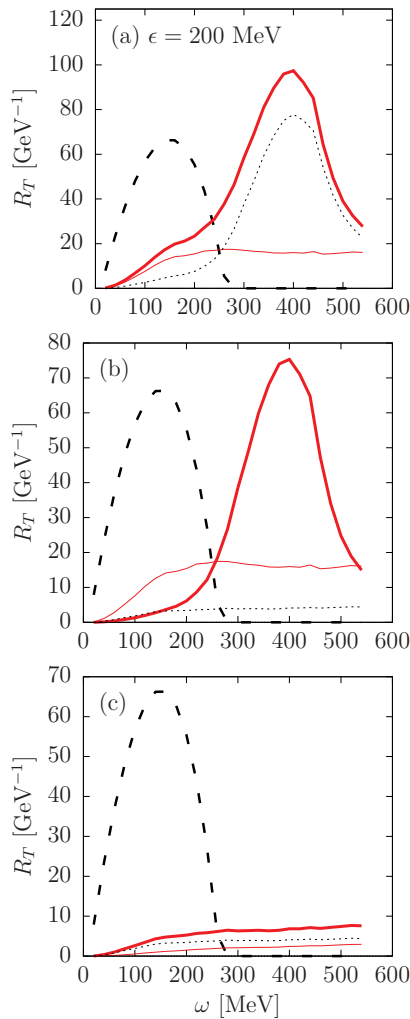
The Δ peak is very small in the longitudinal response presented in Figs. 5 and 6. This is consistent with the predominant transverse character of the Δ current, hence providing a small contribution to the longitudinal channel. For $q = 550$ MeV the MEC 2p-2h contribution is large (small) in the T (L) response. However, for $q = 1140$ MeV (Figs. 4 and 6) we find a larger effect in R_L coming from the MEC seagull and pionic at-large energy transfer. Indeed in a nonrelativistic expansion in powers of q/m_N the time component of the MECs is of higher order than the transverse one. However, for $q = 1140$ MeV, q/m_N is larger than one, and the relative L component of the MECs, compared to the T one, starts to increase.

In the case of the correlation current, we observe that its contribution, compared with the OB responses, is similar in the T and L channels. Note that in the correlation current (Fig. 2) the photon couples directly to a nucleon with the same interaction vertex Γ^μ as the OB current. The other side of the diagram with a pion coupled to a second nucleon is independent of the particular component of the current.

The separate effects of the different currents contributing to the 2p-2h transverse responses are shown in Figs. 9 and 10. As
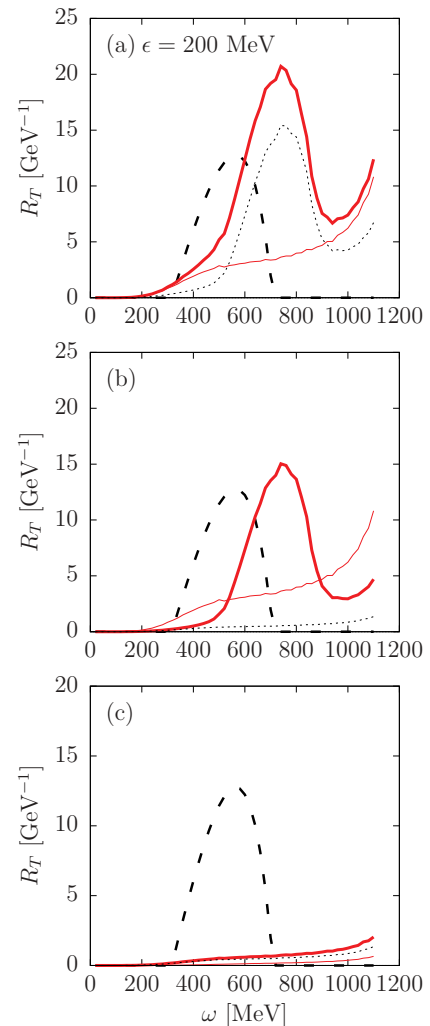

FIG. 9. (Color online) Contributions to the transverse response of ^{56}Fe for $q = 550$ MeV/c. The dashed lines are the 1p-1h response with OB current only. The rest of the lines are 2p-2h contributions. (a) (Top panel) Thin solid, correlation only; dotted, MECs only; thick solid, total. (b) (Middle panel) Thin solid, correlation only; dotted, seagull + pionic only; thick solid, Δ only. (c) (Bottom panel) Thin solid, pion in flight only; dotted, seagull + pionic only; thick solid, seagull only.

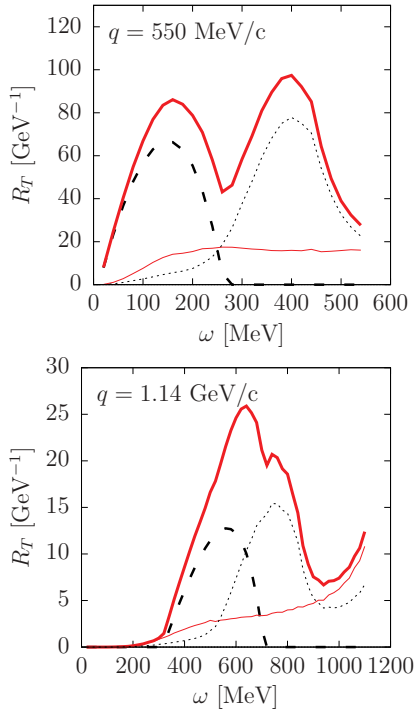FIG. 10. (Color online) The same as for Fig. 9, but now at $q = 1140$ MeV/c.

FIG. 11. (Color online) Transverse response of ^{56}Fe at $q = 550$ and 1140 MeV/c. Thin solid, correlation only for $\epsilon = 200$ MeV; dotted, MECs only; thick solid, total one- plus two- body responses; dashed, RFG 1p-1h response with OB current only.

shown, the seagull plus pionic (SPP) currents alone give a small effect compared with the contributions from the Δ and correlations. In fact, for $\epsilon = 200$ MeV the correlation response is much larger (by a factor 2 or 3) than the SPP response function (middle panels in Figs. 9 and 10). We also observe that the separate seagull contribution is larger in magnitude than the pionic one, which is negligible for $q = 1140$ MeV/c. Note that the two currents interfere destructively and partially cancel when both are considered in the SPP responses (bottom panels).

In Fig. 11 we show the transverse response obtained by adding the total 2p-2h contributions to the OB response. A word of caution should be raised when analyzing these results. First, we have not added the correlation nor MEC corrections to the 1p-1h channel. Moreover, the two-pion-exchange interaction generates self-energy corrections to the OB current that lead to interference effects of the same order in the expansion as the corrections included here. As an example, FSIs are known to redistribute the strength of the responses, producing a hardening, a reduction of the maximum, and an increase of the high-energy tail [20]. Recently, furthermore, a large effect from both MECs and FSIs was found in the 1p-1h channel for high momentum transfer [21], which should be added to the present results. Finally, the process of real pion emission (not included here) also gives a contribution in the transverse response located mainly in the region of the Δ peak.

So far we have presented results for intermediate to high momentum transfer. Results for lower values of $q = 370$ and 410 MeV/c are shown in Figs. 12 and 13 for the T and L response functions. This allows us to compare the present results with previous nonrelativistic calculations [10]. In Fig. 12 the
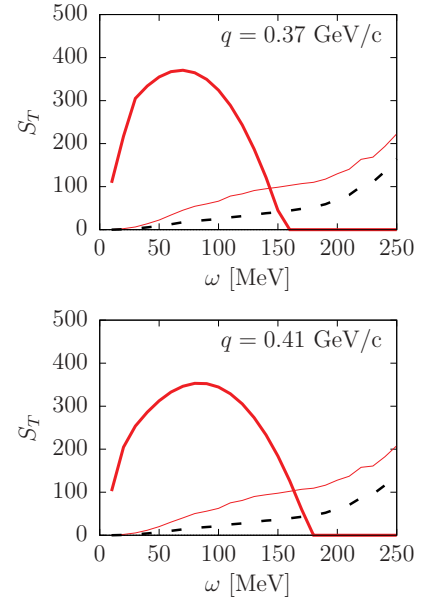

FIG. 12. (Color online) Transverse structure function S_T of ^{56}Fe at $q = 370$ and 410 MeV/c. The parameter $\epsilon = 200$ MeV. To compare with Figs. 11 and 12 of [10], S_T is defined as [22] $S_T = \frac{M_A}{4\pi} R_T$. Thick lines, RFG 1p-1h results; dashed lines, 2p-2h, MECs only; thin solid lines, 2p-2h total, MECs plus correlations.

structure function $S_T = \frac{M_A}{4\pi} R_T$ is presented, to allow a direct comparison with Figs. 11 and 12 of Ref. [10]. The separate MEC and correlation contributions to the 2p-2h T response shown in Fig. 12 are similar to the ones presented in Ref. [10]. The MEC produces a tail above the QE peak that increases with the energy transfer. The presence of correlations leads to an additional, significant rise of the tail. Note that our correlation results are obtained for $\epsilon = 200$ MeV. In Ref. [10] another
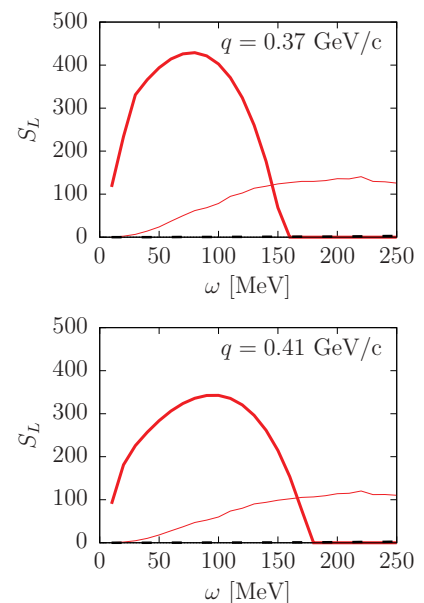

FIG. 13. (Color online) The same as for Fig. 12, but now for the longitudinal structure function $S_L = \frac{M_A}{4\pi} R_L$.

prescription to deal with the nucleon pole was adopted. From our results we conclude that both prescriptions are compatible numerically. The OB response of Ref. [10] included RPA correlations producing a reduction and hardening of the OB response. The 2p-2h longitudinal responses were not computed in Ref. [10], because the time components of the MECs are of higher order in the nonrelativistic reduction and, hence, they were expected to be very small. However, our prediction for the correlation 2p-2h contribution in the L response, presented in Fig. 13, shows a similar effect as in the T response (i.e., a tail also appears for high-energy transfer in the L response coming from correlations). Contrary to the T channel, MECs give no contribution in the L response.

Because the 2p-2h excitation is produced in this work by one-pion exchange, the results are strongly dependent on the details of this particular interaction. This is illustrated in Fig. 14 where we show how the results depend on the strong πNN form factor for $q = 1140$ MeV/c. The results without a form factor (i.e., with $F_{\pi NN} = 1$) are about three times as large as the results with the form factor. This is different from the
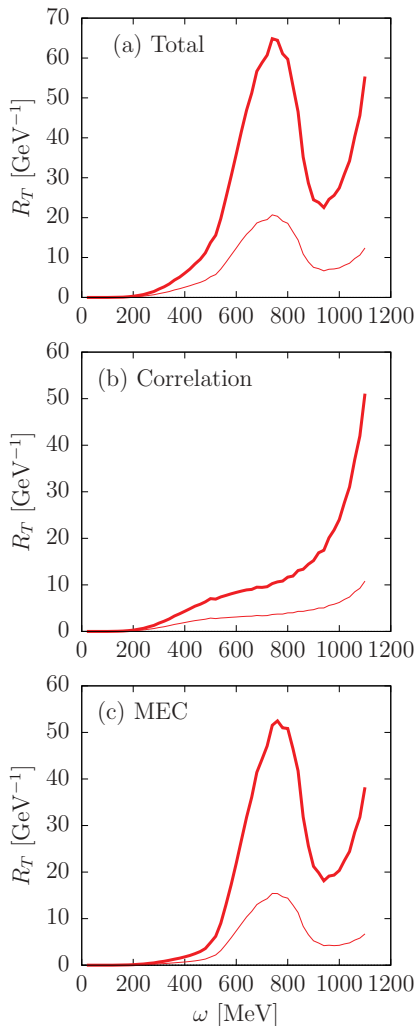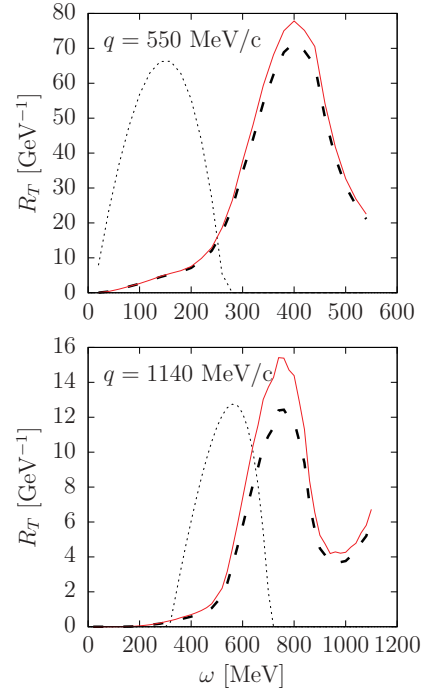

FIG. 15. (Color online) 2p-2h MEC-only contribution to the transverse response of ^{56}Fe. Solid lines, computed with the Δ form factors used by [14]; dashed lines, computed with the Δ form factors used in Ref. [1]; dotted, RFG OB response.

findings at low momentum transfer [9], where the pion form factor can be safely ignored.

Another issue is the dependence of the results on the Δ form factors used in this work, both the electromagnetic and the strong ones, which are somewhat different from the parametrization used in the 2p-2h MEC calculation of Ref. [1]. Calculations done with both sets of parameters are compared in Fig. 15. Our calculation gives a larger contribution for the T response than the one of Ref. [1]. Hence, the use of the same form factors reduces the discrepancy between the two calculations. Some of the remaining differences could be linked to other details of the models, in particular, to the different Lagrangian chosen for Δ electroexcitation. We should note that the two models are fully independent. Although all the spin sums are performed analytically in Ref. [1] resulting in thousands of terms to be numerically integrated, in this work we first compute the spin matrix elements of the current and later we evaluate the squares and perform the sums numerically.

Before concluding, we would like to stress that the 2p-2h responses in the present model are crucially dependent on details of the pion interaction. A critical ingredient of the model is the value of the parameter ϵ, identified with an escape width of a high-energy nucleon from the nucleus. We have proven that a value $\epsilon \sim 200$ MeV leads to results in agreement with the previous calculation of Ref. [10]. This parameter ϵ is different from the usual interaction width of particle states, usually associated with matrix elements of the phenomenological imaginary optical potential derived from elastic scattering data [19]. It was also computed in nuclear matter in a semiphenomenological approach [23]. The resulting width for

FIG. 14. (Color online) 2p-2h T response of ^{56}Fe at $q = 1140$ MeV/c. Thin lines with πNN form factor. Thick lines without form factor ($F_{\pi NN} = 1$). (a) Total; (b) correlations only; (c) MECs only.

100 MeV nucleons is of the order of 10 MeV, which is too small to give reasonable results in our calculation. This is because of the $1/\epsilon$ behavior of the 2p-2h response divergence in the QE region, where the pole is being hit.

Because of this divergent behavior, for $\epsilon = 5$ MeV the results would be almost one order of magnitude larger than the OB responses at the maximum. We have checked that the $1/\epsilon$ term in the forward diagrams is the main contribution to the 2p-2h correlations in the QE region for $\epsilon > 20$ MeV.

The importance of correlations, for the same value of ϵ, increases with the nuclear mass. We have checked that for the case of ^{12}C where the sizes of the correlation responses, relative to the OB, are about 20% smaller than for ^{56}Fe. This is what one would expect, because the number of correlated pairs increases with $A(A-1)/2$. Moreover, because the estimated value of ϵ depends on the nuclear radius, Eq. (37) indicates that one should use larger ϵ values for lighter nuclei, which, in turn, would reduce even more the size of the correlation responses. Thus, we expect an important A dependence of correlations on the nuclear responses coming from the A dependence of the escape width ϵ. A more detailed study of this issue will be presented in forthcoming work.

V. CONCLUSIONS

In this work we have presented a fully relativistic model of inclusive two-particle emission reactions induced by electrons. Starting with the free relativistic Fermi gas we have considered all Feynman diagrams in a perturbative expansion of the scattering amplitude with one-photon and one-pion exchange producing 2p-2h excitations. Those diagrams can be classified in two sets, namely MEC and correlation currents. In the latter there is a nucleon propagator that can be put on shell giving a double pole from $(p_0 - E_{\mathbf{p}} + i\epsilon)^{-2}$ when taking the square of the current matrix element. The corresponding 2p-2h response function diverges as $1/\epsilon$ when $\epsilon \to 0$ plus additional $\ln \epsilon$ terms. Giving a physical meaning to ϵ as the escape width of the nucleus, namely, twice the inverse of the nucleon propagation time, the fact that the corresponding response is infinite is related to the infinite extension of the Fermi gas. Using a finite value of ϵ we account for the finite size of the nucleus, hence, getting a finite result. Having no way to compute ϵ in a Fermi gas, we take it as a parameter. Estimating in a crude way a value around $\sim$200 MeV, we have made an exploratory study of the results as a function of ϵ. The correlation effects decrease with increasing ϵ. Our analysis shows that the assumption $\epsilon \sim$ 200–300 MeV is not unreasonable, whereas for smaller ϵ values the correlation contribution increases significantly in the QE region.

Within this framework we have studied the properties and effects of the different 2p-2h contributions and other ingredients of the model on the transverse and longitudinal response functions of ^{56}Fe for intermediate to high momentum transfer. The MECs give rise to a wide peak in the region of the Δ resonance that dominates the T response. In the L channel the MECs are small for low momentum transfer, but they importantly increase for high momentum above the QE peak where their contribution is of the same size as the OB longitudinal response. Concerning the correlations, they add

to the MECs in the high-energy tail and are of the same order of magnitude. The contribution of the correlations is similar in the L and T responses.

The main goal of this article was to study the effect of 2p-2h pion correlations in the L and T response, analyzing the properties of these effects as a function of a single parameter ϵ. In future work we plan to investigate more physically founded ways to "fine tune" this parameter, including its dependence on kinematics and nuclear species. Finite-size calculations in conjunction with the use of semiphenomenological fits of the nucleon spreading width or fits to existing (e, e') data will also be explored.

APPENDIX A: ISOSPIN MATRIX ELEMENTS

In the model used in this work we compute explicitly the isospin matrix elements of the current operator in the different channels PP (two protons), NN (two neutrons), and PN (proton-neutron) emission.

1. PN channel

We first consider the channel in which we eject a PN pair. In this case there is no symmetry in the wave function and we assume that the first hole is a proton and the second is a neutron (i.e., the initial isospin wave function is $|PN\rangle$). The final state can be $|PN\rangle$ or $|NP\rangle$ depending on if there is or is not charge exchange.

In the case of the MEC seagull and pion in flight, Figs. 1(a)–1(c), this is the only channel that contributes. The isospin operator is

$$U \equiv \epsilon_{3ab} \tau_a^{(1)} \tau_b^{(2)}, \qquad (A1)$$

where repeated indices are meant to be summed. The relevant isospin matrix element is obtained by operating over a PN state,

$$\langle NP|U|PN\rangle = -2i. \qquad (A2)$$

In the case of the correlation current we find four isospin operators for the diagrams of Fig. 2, including the isospin dependence in the single nucleon current Γ^μ, namely,

$$\tau_a^{(1)} \Gamma^{\mu(1)} \tau_a^{(2)}, \qquad \tau_a^{(1)} \tau_a^{(2)} \Gamma^{\mu(2)}, \qquad (A3)$$

$$\Gamma^{\mu(1)} \tau_a^{(1)} \tau_a^{(2)}, \qquad \tau_a^{(1)} \Gamma^{\mu(2)} \tau_a^{(2)}. \qquad (A4)$$

Operating over the initial $|PN\rangle$ state we obtain

$$\tau_a^{(1)} \tau_a^{(2)} \Gamma^{\mu(2)} |PN\rangle = 2\Gamma^{\mu N} |NP\rangle - \Gamma^{\mu N} |PN\rangle, \qquad (A5)$$

$$\tau_a^{(1)} \Gamma^{\mu(2)} \tau_a^{(2)} |PN\rangle = 2\Gamma^{\mu P} |NP\rangle - \Gamma^{\mu N} |PN\rangle, \qquad (A6)$$

$$\tau_a^{(1)}\Gamma^{\mu(1)}\tau_a^{(2)}|PN\rangle = 2\Gamma^{\mu P}|NP\rangle - \Gamma^{\mu P}|PN\rangle, \qquad (A7)$$

$$\Gamma^{\mu(1)}\tau_a^{(1)}\tau_a^{(2)}|PN\rangle = 2\Gamma^{\mu N}|NP\rangle - \Gamma^{\mu P}|PN\rangle. \qquad (A8)$$

In the case of the Δ current, diagrams of Figs. 1 (d)–1(g), we find the following isospin operators:

$$T_3^{(1)}T_a^{\dagger(1)}\tau_a^{(2)}, \qquad T_a^{(1)}T_3^{\dagger(1)}\tau_a^{(2)}, \qquad (A9)$$

$$\tau_a^{(1)}T_a^{(2)}T_3^{\dagger(2)}, \qquad \tau_a^{(1)}T_3^{(2)}T_a^{\dagger(2)}, \qquad (A10)$$

where T_i are the $\frac{3}{2} \to \frac{1}{2}$ isospin transition operators verifying

$$T_i T_J^{\dagger} = \frac{2}{3}\delta_{ij} - \frac{i}{3}\epsilon_{ijk}\tau_k. \qquad (A11)$$

For instance, we have

$$T_a^{(1)}T_3^{\dagger(1)}\tau_a^{(2)} = \frac{2}{3}\tau_z^{(2)} - \frac{i}{3}[\boldsymbol{\tau}^{(1)} \times \boldsymbol{\tau}^{(2)}]_z, \qquad (A12)$$

$$T_3^{(1)}T_a^{\dagger(1)}\tau_a^{(2)} = \frac{2}{3}\tau_z^{(2)} + \frac{i}{3}[\boldsymbol{\tau}^{(1)} \times \boldsymbol{\tau}^{(2)}]_z, \qquad (A13)$$

and similarly changing $1 \leftrightarrow 2$. Operating over the initial $|PN\rangle$ state we obtain

$$T_a^{(1)}T_3^{\dagger(1)}\tau_a^{(2)}|PN\rangle = -\tfrac{2}{3}|NP\rangle - \tfrac{2}{3}|PN\rangle, \qquad (A14)$$

$$T_3^{(1)}T_a^{\dagger(1)}\tau_a^{(2)}|PN\rangle = \tfrac{2}{3}|NP\rangle - \tfrac{2}{3}|PN\rangle, \qquad (A15)$$

$$\tau_a^{(1)}T_a^{(2)}T_3^{\dagger(2)}|PN\rangle = \tfrac{2}{3}|NP\rangle + \tfrac{2}{3}|PN\rangle, \qquad (A16)$$

$$\tau_a^{(1)}T_3^{(2)}T_a^{\dagger(2)}|PN\rangle = -\tfrac{2}{3}|NP\rangle + \tfrac{2}{3}|PN\rangle. \qquad (A17)$$

2. *PP* channel

In the case of two-proton emission only the Δ and correlation diagrams contribute. In the case of the correlations, the isospin operators over the initial $|PP\rangle$ state give

$$\tau_a^{(1)}\tau_a^{(2)}\Gamma^{\mu(2)}|PP\rangle = \Gamma^{\mu P}|PP\rangle, \qquad (A18)$$

and exactly the same result for the remaining three operators.

In the case of the Δ we have

$$T_a^{(1)}T_3^{\dagger(1)}\tau_a^{(2)}|PP\rangle = \tfrac{2}{3}|PP\rangle, \qquad (A19)$$

and exactly the same answer for the remaining three operators.

3. *NN* channel

Once more only the Δ and correlation diagrams contribute. In the case of the correlations, we have

$$\tau_a^{(1)}\tau_a^{(2)}\Gamma^{\mu(2)}|NN\rangle = \Gamma^{\mu N}|NN\rangle, \qquad (A20)$$

and the same for the remaining three operators.

Finally, for the Δ we have

$$T_a^{(1)}T_3^{\dagger(1)}\tau_a^{(2)}|NN\rangle = -\tfrac{2}{3}|NN\rangle, \qquad (A21)$$

and the same answer again for the remaining three operators.

APPENDIX B: INTEGRATION OF THE ENERGY δ FUNCTION

The 9D integral for the 2p-2h response functions is of the type,

$$\int d^3p_1' d^3h_1 d^3h_2 \delta(E_1 + E_2 + \omega - E_1' - E_2') f(\mathbf{h}_1, \mathbf{h}_2, \mathbf{p}_1', \mathbf{p}_2'),$$
$$(B1)$$

where $\mathbf{p}_2' = \mathbf{h}_1 + \mathbf{h}_2 + \mathbf{q} - \mathbf{p}_1'$. The δ function allows us to perform one integration analytically imposing energy conservation. Therefore, for fixed values of the two-hole momenta $\mathbf{h}_1$, $\mathbf{h}_2$ and for fixed values of the two emission angles θ_1', ϕ_1' of particle 1, we can integrate over the momentum p_1', fixing the energy of the first particle. To this end, we change variables $p_1' \to E' = E_1' + E_2'$. Taking into account that both energies E_1' and E_2' depend on p_1' to compute the Jacobian of the transformation, we obtain

$$dp_1' = \frac{dE'}{\left| \frac{p_1'}{E_1'} - \frac{\mathbf{p}_2' \cdot \mathbf{p}_1'}{E_2' p_1'} \right|}, \qquad (B2)$$

where the momentum of the final nucleon for fixed emission angles θ_1', ϕ_1' is obtained by solving the energy conservation equation. This is a second-degree equation with two solutions given explicitly by

$$p_1' = \frac{a}{b}\left(v \pm v_0 \sqrt{1 - \frac{bm_N^2}{a^2}} \right), \qquad (B3)$$

where

$$a = \tfrac{1}{2}p'^2, \qquad (B4)$$

$$b = E'^2 - p'^2 \cos^2\beta_1', \qquad (B5)$$

$$v_0 = E', \qquad (B6)$$

$$v = p' \cos\beta_1'. \qquad (B7)$$

$E' = E_1 + E_2 + \omega$ is the final total energy, $\mathbf{p}' = \mathbf{h}_1 + \mathbf{h}_2 + \mathbf{q}$ is the final total momentum, and β_1' is the angle between $\mathbf{p}_1'$ and $\mathbf{p}'$. To compute the integral we add the contributions from these two solutions, corresponding to two possible final states compatible with energy-momentum conservation.

[1] A. De Pace, M. Nardi, W. M. Alberico, T. W. Donnelly, and A. Molinari, Nucl. Phys. A **726**, 303 (2003).

[2] A. De Pace, M. Nardi, W. M. Alberico, T. W. Donnelly, and A. Molinari, Nucl. Phys. A **741**, 249 (2004).

[3] J. W. Van Orden and T. W. Donnelly, Ann. Phys. **131**, 451 (1981).

[4] M. J. Dekker, P. J. Brussaard, and J. A. Tjon, Phys. Lett. B **266**, 249 (1991).

[5] M. J. Dekker, P. J. Brussaard, and J. A. Tjon, Phys. Lett. B **289**, 255 (1992).

[6] M. J. Dekker, P. J. Brussaard, and J. A. Tjon, Phys. Rev. C **49**, 2650 (1994).

[7] M. J. Dekker, P. J. Brussaard, and J. A. Tjon, Phys. Rev. C **49**, 2650 (1994).

[8] J. E. Amaro, G. Co, and A. M. Lallena, Ann. Phys. (NY) **221**, 306 (1993).

[9] J. E. Amaro, G. Co, and A. M. Lallena, Nucl. Phys. A **578**, 365 (1994).

[10] W. M. Alberico, M. Ericson, and A. Molinari, Ann. Phys. (NY) **154**, 356 (1984).

[11] W. M. Alberico, A. de Pace, A. Drago, and A. Molinari, Riv. Nuovo Cimento **14**, 1 (1991).

[12] A. Gil, J. Nieves, and E. Oset, Nucl. Phys. A **627**, 543 (1997).

[13] J. E. Amaro, M. B. Barbaro, J. A. Caballero, T. W. Donnelly, and A. Molinari, Phys. Rep. **368**, 317 (2002).

[14] J. E. Amaro, M. B. Barbaro, J. A. Caballero, T. W. Donnelly, and A. Molinari, Nucl. Phys. A **723**, 181 (2003).

[15] J. D. Bjorken and S. D. Drell, *Relativistic Quantum Mechanics (Pure & Applied Physics)* (McGraw-Hill Inc., US, 1965).

[16] V. Pascalutsa and O. Scholten, Nucl. Phys. A **591**, 658 (1995).

[17] S. Galster *et al.*, Nucl. Phys. B **32**, 221 (1971).

[18] F. Mandl and G. Shaw, *Quantum Field Theory* (John Wiley & Sons Inc., 1984).

[19] R. D. Smith and J. Wambach, Phys. Rev. C **38**, 100 (1988).

[20] J. E. Amaro, M. B. Barbaro, J. A. Caballero, T. W. Donnelly, and J. M. Udias, Phys. Rev. C **75**, 034613 (2007).

[21] J. E. Amaro, M. B. Barbaro, J. A. Caballero, T. W. Donnelly, C. Maieron, and J. M. Udias, Phys. Rev. C **81**, 014606 (2010).

[22] J. S. McCarthy, Nucl. Phys. A **335**, 27 (1980).

[23] P. Fernandez de Cordoba and E. Oset, Phys. Rev. C **46**, 1697 (1992).